21st Australasian Fluid Mechanics Conference
Adelaide, Australia
10-13 December 2018

One-way and Two-way Coupled PDF-PBE/LES Simulations of Turbulent Particle-Laden Flows

F. Salehi[1], M. J. Cleary[2], A. R. Masri[2] and A. Kronenburg[3]

[1]School of Engineering
Macquarie University, NSW 2109, Australia

[2]School of Aerospace, Mechanical and Mechatronics Engineering
The University of Sydney, NSW 2006, Australia

[3]Institut für Technische Verbrennung
Universität Stuttgart, Herdweg 51, 70174 Stuttgart, Germany

Abstract

This paper studies the influence of the fluid-particle interaction for the prediction of turbulent particle-laden flows in a bluff body configuration. The simulations are performed using a probability density function form of the population balance equation (PDF-PBE) in the large eddy simulation (LES) context. The inertia of particles of different sizes is effectively modelled using a newly developed Stokes binning method which divides the PDF-PBE into classes based on the particle Stokes numbers. A two-way coupling is applied considering the interaction between the continuous and particulate phase only by momentum exchange terms. The studied case is an experiment of glass beads injected into a recirculating flow. Good agreement is observed between the simulations and the measurements. The results also confirm that the flow field of the continuous phase is influenced by the particulate phase and this is consistent with the experimental observations.

Introduction

Turbulent flow fields laden with particles much heavier than the gas phase occur in a wide range of engineering and environmental applications. The interactions between partly responsive particles and turbulent flows imply a lot of interdependent effects where the evolution of the dispersed phase and the carrier phase are, in general, coupled. Detailed computational modelling of such flows will provide a better understating and eventually improve the design of engineering devices from combustion chambers and engines to drug delivery systems.

The population balance equation (PBE) [13] has been widely used for the particulate flows. The PBE presents the evolution of the number density function in coordinate space and also property space which can include droplet size (commonly, volume), shape, surface area, morphology, etc. Rigopoulos [11] introduced a probability density function (PDF) form of the PBE for turbulent dispersions and these have been widely applied to the modelling of non-inertial elements for processes such as droplet nucleation and growth, particle synthesis and particle aggregation [10, 11, 14, 6]. Recently, the PDF-PBE approach was extended for inertial polydispersed and polyshaped particle-laden flows [12]. The model was numerically tested and also validated against experimental data for droplet dispersion in the one-way coupled regime in which the dispersed elements have negligible effect on the carrier phase.

The present work employs the inertial PDF-PBE model to study effects of the momentum coupling. The experiment of Boree et al. [2] is selected here where the evolution of polydispersed glass beads in a complex, recirculating flow was investigated. Previously, both RANS [5] and LES [9, 1] methods were employed for numerical investigation of this configuration. Minier et al. [5] used a stochastic Lagrangian approach in a RANS framework and showed a satisfactory agreement between simulations and measurements although the locations of the stagnation points were shifted downstream. Alletto and Breuer [1] performed LES-Lagrangian simulations and presented results computed based on one-way and two-way couplings, confirming the significant impact of momentum coupling on the results. Riber et al. [9] performed two-way coupled LES for 60 μm particles as the representative size. The results agreed well with the experiment while some deviations were found and predominantly attributed to uncertainties in the boundary conditions.

Here, we consider dispersion of multiple glass bead sizes at the 22% mass loading and compare the results with the available experimental data. Further analysis is also performed to provide more insight on the effect of momentum coupling. The impact of particle inlet boundary conditions is also investigated.

PDF-PBE

The evolution of the instantaneous particle number density, n, in the coordinate space, $\boldsymbol{x} = (x_1, x_2, x_3)$, and the property (or state) space, $\boldsymbol{\xi} = (\xi_1, ..., \xi_M)$ is governed by the PBE [13]

$$\frac{\partial n}{\partial t} + \nabla_{\boldsymbol{x}} (\boldsymbol{u} n) + \nabla_{\boldsymbol{\xi}} \left(\dot{\boldsymbol{\xi}} n \right) = w, \tag{1}$$

where $\boldsymbol{u}(\boldsymbol{\xi}; \boldsymbol{x}, t)$ is the velocity in physical space, $\dot{\boldsymbol{\xi}}(\boldsymbol{\xi}; \boldsymbol{x}, t)$ is the velocity in the property space representing processes such as condensation and evaporation, and w is the source term representing processes such as breakages and agglomeration. For this study, the property space includes only the particle volume so that $\boldsymbol{\xi} = \xi_1 = V$ and w and $\dot{\boldsymbol{\xi}}$ are neglected.

The PDF form of Eq. 1 is considered here and it is recast in stochastic form and solved using Lagrangian notional particles in a Monte Carlo simulation. An accurate model for effects of inertia is essential since all dispersed element sizes with their vastly different slip velocities and trajectories cannot be represented on each notional particle. Here, the PDF-PBE is divided into classes, where each class represents the turbulent distribution of the number density function of dispersed elements that have similar inertial interactions with the carrier phase [12]. The stochastic differential equations for each class of notional particles can be written as

$$\begin{aligned} d\boldsymbol{X} &= \boldsymbol{U} dt \\ d\boldsymbol{U} &= \boldsymbol{A} dt, \end{aligned} \tag{2}$$

where $\boldsymbol{X}$ is the notional particle position while $\boldsymbol{U}$ and $\boldsymbol{A}$ are the velocity and the acceleration, respectively. The drag is the dominant accelerating force on the particles and hence the acceleration, $\boldsymbol{A}$, can be written as [4]

$$d\boldsymbol{U} = \frac{1}{<\tau_p>}(\boldsymbol{v}-\boldsymbol{U})\,dt, \tag{3}$$

where $<\tau_p>$ is the mean (across the class) response time due to carrier and dispersed phase interaction forces. If each PDF-PBE class is limited to solid elements of only one size then $<\tau_p>=\tau_p=\tau_p(\boldsymbol{\xi};x,t)$ which is modelled as

$$\frac{1}{\tau_p} = \frac{1}{2}C_D\frac{\rho}{\rho_d}\frac{A_d}{V_d}|\boldsymbol{v}-\boldsymbol{U}|, \tag{4}$$

where C_D is the drag coefficient, ρ is the carrier fluid density, ρ_d is the dispersed phase density, A_d is a reference area and V_d is the dispersed element volume. The instantaneous carrier velocity at the notional particle location is obtained using the Langevin model [8]. More details are provided in [12].

For the mass loading of 22% considered here, the glass bead volume fraction is 1×10^{-4} and the influence of the dispersed phase on the carrier phase is therefore important [1]. The momentum coupling source term in the momentum equation of the carrier phase represents this effect. The source term is modelled by a summation over the entire ensemble of notional particles [3].

The method of Stokes binning

The selection of the PDF-PBE classes should ensure that they represent the physical dispersed elements with similar effects of inertia. This is done based on the Stokes binning method [12]. The Stokes number is defined as $St=\tau_p/\tau_f$ where τ_p is the dispersed element response time given by Eq. 4 and τ_f is the fluid characteristic time scale that expresses the response of an inertial element to changes in the carrier flow. This method assumes that particles within a narrow range of Stokes numbers, of width ΔSt, have approximately the same dynamic response to variations in the carrier phase. The Stokes bin size, ΔSt, therefore determines the maximum range of inertial responses represented by the PDF-PBE classes. Notional particles are allocated into classes dynamically, and if necessary may be split into two or more parts. If dSt represents the range of Stokes numbers of inertial elements represented by a notional particle then $dSt\leqslant\Delta St$ is the criterion by which the dynamic selection is made. dSt is a time-dependent variable associated with a specific notional particle and here it varies as the slip velocity changes, while ΔSt is constant and selected prior to simulations. The acceleration of a notional particle is then determined by the average response time, $<\tau_p>$, calculated over the dispersed elements represented by that notional particle. In line with our earlier findings, here we employ eight Stokes bins with $\Delta St=0.38$ [12].

Experimental and numerical set-up

The experimental case studied the dispersion of polysized spherical glass particles downstream of a confined bluff body. The inner pipe with a radius of $R_i=10$ mm is centred in a bluff-body (radius R_b = 75 mm) which itself is centred in a chamber ($R_a=150$ mm). The mean velocities at the inner pipe and the annular ring are $\bar{v}_i$ =3.4 m/s and $\bar{v}_a$ =4.1 m/s, respectively. Two stagnation points were observed in the recirculation region for the single-phase mode. Glass beads are injected in the conducting pipe of the inner jet. These beads have a density of $\rho_d=2470$ kgm^{-3} and diameters varying in the range of 20 to 100 μm with a constant size interval of 10 μm. The mass and number distribution of glass beads at the inlet can be found in Ref. [2]. The mass loading in the inner pipe is 22% where the impact of solid particles on the carrier phase is important.

The PDF-PBE is implemented into OpenFOAM while a standard low-Mach compressible spatially and temporally second-order LES solver of OpenFOAM is adopted. The subgrid stress tensor is modelled using the Wall-Adapting Local Eddy-viscosity (WALE) model [7]. A tri-linear interpolation is employed to compute the carrier phase velocities, density, and turbulent kinematic energy at the particle locations.

The cylindrical computational domain has a diameter of 300 mm and a length of 800 mm. The grid resolution in the inner jet, over the bluff body and in the annulus region is efficiently controlled by a quad-dominant unstructured sweeping method. The mesh has approximately 4M cells with a cell size of 0.7 mm at the inner jet and 1 mm near the annulus and bluff-body. No-slip conditions are imposed at the walls. Non-reflective pressure zero gradient pressure boundary conditions are applied at the outlet and the inlets, respectively. Time-varying realistic turbulent velocity boundary conditions are used for both inner and annular jets. In a pre-processing step, two separate pipe LES simulations with the same cross sections as the inner and annular sections are performed to generate accurate and realistic inner jet and annulus inflow velocities.

At injection, a notional particle represents a range of glass bead sizes such that their inlet Stokes numbers ($St_{inlet}=\rho_d d_p^2/18\mu\tau_f$) satisfy the Stokes binning criterion $dSt\leqslant\Delta St$. Notional particles are injected at $z=0$ whereas their inlet x and y locations are randomly selected on the inner jet plane. The introduction of the particle velocities is one of the main difficulty in such a two-phase flow configuration. The most accurate method could be pre-processing a realistic two-phase pipe simulation where particle-particle interactions and the effect of the rough pipe walls on particles should be modelled [1]. However, these are expensive and lower cost and simpler methods are required. The simplest approach is associating the carrier velocity to an injected notional particle, however, neglecting the inertial effects at the injection may significantly affect the particle trajectories with different sizes. Another solution is using the mean velocity profiles provided by the experiment [2] at $z=3$ mm. Each notional particle mean velocity is computed by averaging over the experimental mean velocities for size distribution it represents and a white noise is also added to the mean value [9]. Here, we test the impact of particle boundary conditions at the inlet. For this purpose, the simulations are performed where (i) the carrier phase velocity is assigned into an injected notional particle ($U_{\text{inj}}=V$), (ii) the velocity of an injected notional particle is computed based on the profiles of measured particle mean velocities ($U_{\text{inj}}=U_{\text{Exp}}$) and (iii) a level of randomness is imposed into the mean experimental value. As suggested in Ref. [9], we use a white noise with an amplitude of the order of 10% of the mean velocity ($U_{\text{inj}}=U_{\text{Exp}}+10\%$). A value of 5% of the mean velocity ($U_{\text{inj}}=U_{\text{Exp}}+5\%$) is also tested here.

Results and discussion

Particle boundary conditions

Figure 1 presents the evolution of the particle mean axial velocity and its root mean square (RMS) along the centreline for 60 μm particles. The measurements are shown by filled red symbols whereas the two-way coupled simulation results are illustrated by lines and symbols. Generally, good agreement is found between PDF-PBE results and the experiment. The predicted mean velocities decay faster than the experiment, resulting in higher RMS values before the inner jet stagnation point and consequently shifting the location of the peak RMS slightly ahead of the experiment. Further downstream, the mean and RMS values are in good agreement with the measurements. The

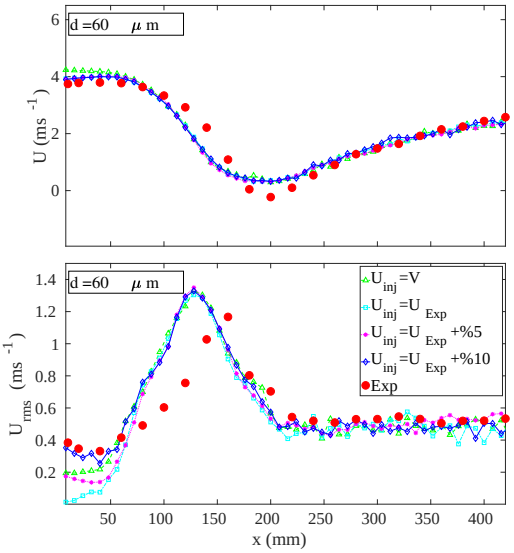

Figure 1: Particle mean axial velocity along the centreline for 60 μm particles.

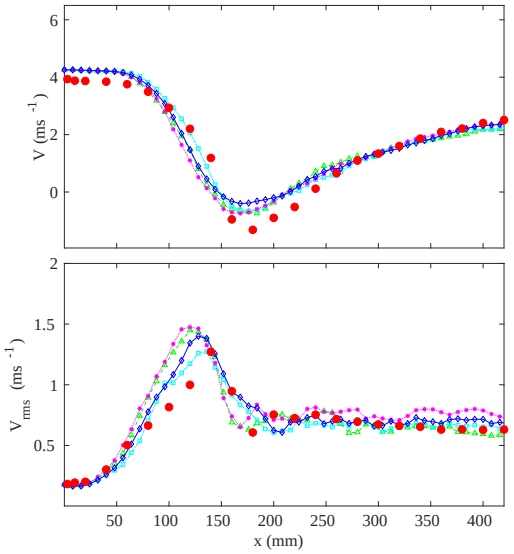

Figure 2: Carrier mean axial velocity along the centreline - effects of boundary conditions.

results demonstrate the effects of inlet boundary conditions for particles is only important at the early stage. The particle mean axial velocity is initially over-predicted when the notional particles are injected with the carrier patch velocity. Other models do not reveal any significant differences and they show good agreement with the experiment. The impact of boundary conditions becomes more significant on the particle velocity RMS. It can be seen that the PDF-PBE reproduces the early decrease in RMS values very well when a level of randomness is imposed into the particle injection velocity. Similarly, further downstream the effect of inlet conditions becomes marginal.

Figure 2 shows the mean axial carrier velocity and its RMS along the centreline. The legend is same as Fig. 1. Overall, the agreement between the PDF-PBE results and the experiment is satisfactory. The two stagnation points where the axial velocity becomes zero are captured well. The two-way coupled results show that the location of the inner jet stagnation point agrees well with the experiment whereas the second stagnation point is upstream of the measurement. The evolution of the velocity RMS is well captured by simulations and, in particular, the location of the peak RMS near the inner stagnation point is accurately predicted. However, the simulations reveal slightly higher peak velocity RMS values. It can be seen that small changes in the inlet boundary conditions of particles have a significant impact on the carrier phase, confirming the importance of the momentum coupling. As expected, initially the effect of boundary conditions on the carrier mean velocity and its RMS is negligible although it becomes important, particularity near the jet breakup point. Imposing a level of randomness into the initial particle velocity leads to a faster decay of the carrier mean velocity and hence shifting the location of the peak RMS slightly ahead of the experiment. Considering both particle and carrier velocities, it may be concluded that the best agreement between the PDF-PBE and the experiment is achieved when the injection velocity for particles is obtained using an imposed white noise with an amplitude of the order of 10% of the mean velocity into the mean measured velocity profiles.

Momentum coupling

To highlight the impact of the dispersed elements on the carrier phase, the simulations were also performed while the momentum source term was set to zero. The results (carrier phase velocities) are presented in Fig. 3. The one-way coupled results are presented by dashed green lines and should be compared with the single-phase experimental data shown by filled green symbols. For comparison purposes, we also present the two-way coupled simulations in which the velocity of injected notional particles are computed using an imposed white noise with an amplitude of the order of 10% of the mean velocity into the mean measured velocity profiles. Solid red lines and filled red symbols show the two-way coupled results and the measurements of the two-phase flows, respectively. The one-way coupled simulation predicts the location of both stagnation points and the evolution of carrier phase velocity RMS very well. The results clearly reveal the impact of the dispersed elements on the carrier phase and this is in agreement with the experimental data. Similar to the measurements, the two-way coupled results show a slower decay of the axial velocity compared to the one-way coupled results before the first stagnation point. The single-phase measured velocities are moderately larger than the two-phase measurements at $x > 180$ mm however, the difference between one-way and two-way coupling simulations is small for locations downstream the second stagnation point.

Figure 4 presents the mean distance from the centreline for 60 μm particles at axial locations of $z = 80$, 160, 240, 320 and 400 mm. It should be noted that the experimental data is only available for 60 μm particles. The trend of particles dispersion in the present flow configuration is significantly different from polydisperse round jet flows and this is due to the existence of a strong recirculation zone. The level of particle dispersion along the centreline initially decreases and reaches its minimum value near the first stagnation point and then slightly increases downstream of this point before reaching a steady value. The PDF-PBE reproduces the dispersion of 60 μm particles very well at all axial locations except $z = 80$ mm where the dispersion is slightly under-predicted. The particle dispersion is also computed using the one-way coupled results and presented in Fig. 4 by green lines. The one-way coupled simulation reveals a similar level of dispersion at all axial locations except at $x = 160$ mm. This is due to the significant difference in the carrier flow field in the one-way and two-way coupled simulations near the stagnation point as shown in Fig. 3. The recirculation zone is

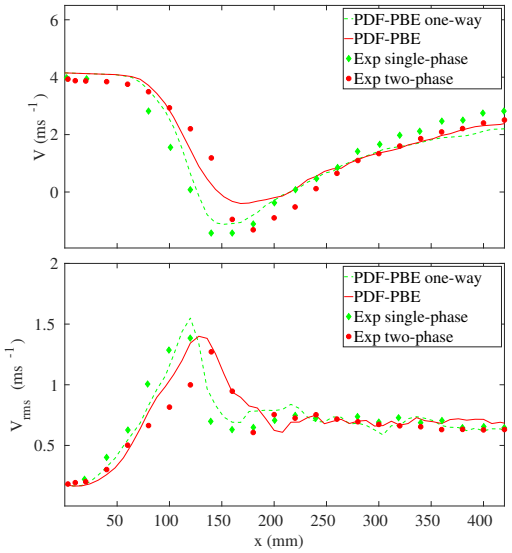

Figure 3: Carrier mean axial velocity along the centreline - effects of momentum coupling.

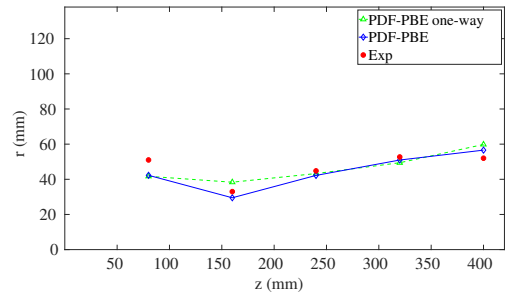

Figure 4: Mean radial dispersion for 60 μm particles as a function of axial location.

larger when the interphase momentum source is neglected and hence the particles radially disperse more compared to the condition where the carrier momentum is affected by the inertial elements.

Conclusion

The PDF-PBE simulations were presented for the experiment of dispersion of inertial polydispersed particles in a bluff-body configuration [2]. Large eddy simulation was employed for the carrier fluid whereas a stochastic version of the PDF-PBE was adopted for the dispersed phase. The cases studied here included particles in the size range of 20-100 μm injected with a mass loading of 22% for which the impact of dispersed elements on carrier phase was significant. The results showed good agreement between the PDF-PBE and measurements. Four different particle inlet boundary conditions were tested. It was found that the particle velocity injection initially affected the evolution of both particles and the carrier phase velocities however, further down stream this impact was faded. To study momentum coupling effects, one-way coupled simulations were also performed in which the source term in the carrier-phase momentum equation was set to zero. The results revealed the strong impact of momentum coupling, particularly on the carrier phase.

Acknowledgements

The work is funded by the Australian Research Council (ARC). FS, MJC and AK acknowledge the financial support provided by Universities Australia and Deutscher Akademischer Austausch Dienst (UA-DAAD). The authors acknowledge the HPC service at the University of Sydney and AWS service funded by Macquarie University for providing computing resources.

References

[1] Alletto, M. and Breuer, M., One-way, two-way and four-way coupled LES predictions of a particle-laden turbulent flow at high mass loading downstream of a confined bluff body, *Int, J. Multiphase Flow*, **45**, 2012, 70 – 90.

[2] Borée, J., Ishima, T. and Flour, I., The effect of mass loading and inter-particle collisions on the development of the polydispersed two-phase flow downstream of a confined bluff body, *J. Fluid Mech.*, **443**, 2001, 129–165.

[3] Galindo-Lopez, S., Salehi, F., Cleary, M. J., Masri, A. R., Neuber, G., Stein, O. T., Kronenburg, A., Varna, A., Hawkes, E. R., Sundaram, B. et al., A stochastic multiple mapping conditioning computational model in openfoam for turbulent combustion, *accepted for publication in Comput. Fluids, doi:10.1016/j.compfluid.2018.03.083*.

[4] Maxey, M. R. and Riley, J. J., Equation of motion for a small rigid sphere in a nonuniform flow, *Phys. Fluids (1958-1988)*, **26**, 1983, 883–889.

[5] Minier, J.-P., Peirano, E. and Chibbaro, S., Pdf model based on langevin equation for polydispersed two-phase flows applied to a bluff-body gas-solid flow, *Phys Fluids*, **16**, 2004, 2419–2431.

[6] Neuber, G., Kronenburg, A., Stein, O. and Cleary, M., MMC-LES modelling of droplet nucleation and growth in turbulent jets, *Chem. Eng. Sci.*, **167**, 2017, 204–218.

[7] Nicoud, F. and Ducros, F., Subgrid-scale stress modelling based on the square of the velocity gradient tensor, *Flow turbul. Combust.*, **62**, 1999, 183–200.

[8] Pozorski, J. and Apte, S. V., Filtered particle tracking in isotropic turbulence and stochastic modeling of subgrid-scale dispersion, *Int. J. Multiphase Flow*, **35**, 2009, 118–128.

[9] Riber, E., Moureau, V., García, M., Poinsot, T. and Simonin, O., Evaluation of numerical strategies for large eddy simulation of particulate two-phase recirculating flows, *J. Comput. Phys.*, **228**, 2009, 539–564.

[10] Rigopoulos, S., PDF method for population balance in turbulent reactive flow, *Chem. Eng. Sci.*, **62**, 2007, 6865–6878.

[11] Rigopoulos, S., Population balance modelling of polydispersed particles in reactive flows, *Prog. Energy Combust. Sci.*, **36**, 2010, 412–443.

[12] Salehi, F., Cleary, M. J. and Masri, A. R., Population balance equation for turbulent polydispersed inertial droplets and particles, *J. Fluid Mech.*, **831**, 2017, 719–742.

[13] Sporleder, F., Borka, Z., Solsvik, J. and Jakobsen, H. A., On the population balance equation, *Rev. Chem. Eng.*, **28**, 2012, 149–169.

[14] Vo, S., Kronenburg, A., Stein, O. T. and Cleary, M. J., Multiple mapping conditioning for silica nanoparticle nucleation in turbulent flows, *Proc. Combust. Inst.*, **36**, 2017, 1089–1097.